# Nature of the superconducting fluctuations in photoexcited systems

Ryuta Iwazaki [1], Naoto Tsuji,[2] and Shintaro Hoshino[1]

[1]*Department of Physics, Saitama University, Shimo-Okubo, Saitama 338-8570, Japan*
[2]*RIKEN Center for Emergent Matter Science (CEMS), Wako, Saitama 351-0198, Japan*

The photoexcited state associated with superconducting fluctuations above the superconducting critical temperature $T_c$ is studied based on the time-dependent Ginzburg-Landau approach. The excited state is created by an electric-field pulse and is probed by a weak secondary external field, which is treated by the linear response theory mimicking pump-probe spectroscopy experiments. The behavior is basically controlled by two relaxation rates: one is $\gamma_1$ proportional to the temperature measured from the critical point $T - T_c$, and the other is $\gamma_2$ proportional to the excitation intensity of the pump pulse. The excited state approaches the equilibrium state exponentially in a long time $t \gg \gamma_1^{-1}$, while in the intermediate-time domain we find a power-law or logarithmic decay with different exponents for $t \ll \gamma_2^{-1}$ and $\gamma_2^{-1} \ll t \ll \gamma_1^{-1}$, even though the system is located away from the critical point. This is interpreted as the critical point in equilibrium being extended to a finite region in the excited situation. The parameter dependences on both the pump and probe currents are also systematically studied in all dimensions.

## I. INTRODUCTION

Externally excited systems can show various exotic states that are not realizable as equilibrium states but nevertheless survive for a long time in nonequilibrium. Such a possibility has been intensively studied by pump-probe experiments using a laser pulse, and the intriguing photoexcited states have been created and measured [1–8]. For superconducting materials in strongly correlated systems, recent experiments have shown gigantic enhancement of superconductivity in a photoinduced state [4,9–15], which has attracted considerable attention in the physics community. While the change in the electron-phonon coupling through the phonon drive has been studied as the origin of the photoinduced superconducting state [16–26], photons also pump the electrons directly. Some of the theoretical studies have proposed scenarios based on photoexcited electron systems [27,28].

The superconductivity-like behavior above the transition temperature $T_c$ is reminiscent of paraconductivity originating from the fluctuation effects: the electron conduction near the superconducting transition point becomes much higher than in the normal state. Usually, the superconducting fluctuation is so small in three-dimensional systems that it has been mainly discussed in low-dimensional systems [29]. With excitations, however, the fluctuation effects may change. Here, we study such a photoinduced phenomenon associated with the superconducting fluctuation based on the time-dependent (TD) Ginzburg-Landau (GL) approach.

The GL theory has been successfully applied to unconventional superconductors [30]. In the strongly correlated systems, since the coherence length can be an order of a lattice constant, the application of GL analysis may not be justified but still describes well their qualitative behaviors. This indicates that extrapolation from the long-wavelength (coherence length) limit works well for existing superconductors. As for

the time-dependent case, it is argued that the TDGL equation is not microscopically justified for gapped superconductors, because the relaxation time of quasiparticles can become longer than the time scale of the order parameter variation [31,32]. The microscopic theory can support the TDGL model for the gapless limit associated with various mechanisms by magnetic impurities, inelastic phonon scattering, or by nonmagnetic impurities for unconventional superconductors [32]. On the other hand, once the TDGL equation is empirically introduced as a phenomenological theory, it has been recognized as a powerful tool for time-dependent phenomena such as vortex dynamics and fluctuation paraconductivity/diamagnetism [29,32]. Furthermore, specifically for the paraconductivity defined in $T > T_c$, the TDGL approach with a stochastic force reasonably reproduces the microscopically calculated Aslamasov-Larkin contribution [29].

The TDGL theory has been applied to the pump-probe spectroscopy below the transition temperature [27]. With a fast pump process in real time, a broad range of frequency components are excited. The TDGL equation can account for the dynamics of small-frequency components, which should dominate the long-time behavior. In this paper, we consider the superconducting fluctuation effects in the photoexcited state using the TDGL equation above the transition temperature, and the behaviors in the whole time scale can be uniquely determined. The quench dynamics of superconducting fluctuations with a sudden change of an attractive interaction has been discussed in Ref. [33]. We consider here purely electronic effects in photoexcited systems. The original paper by Schmid has derived the fluctuation-induced current for arbitrary strength of electric fields [34]. Also, recently the nonlinear response was considered in relation to the nonreciprocal transport phenomena in noncentrosymmetric systems [35–37]. Thus the TDGL theory has the ability to tackle the problem beyond the usual linear-response regime.

When we apply the strong electric-field pulse, there are two characteristic inverse-time scales $\gamma_1$ and $\gamma_2$. $\gamma_1$ originates from the reduced temperature measured from the critical temperature $T_c$, and it determines a time constant for the relaxation into the equilibrium state. The other one, $\gamma_2$, comes from the strength of the electric-field pulse. We show that for $t \to \infty$, the system relaxes to the equilibrium state with the time constant $\gamma_1^{-1}$, but in the intermediate time domain the power-law or logarithmically decaying regimes are found. The exponents are different between the time regions $t \ll \gamma_2^{-1}$ and $t \gg \gamma_2^{-1}$. As for the conductivity calculated from the probe current, the enhancement by the pulse is not observed. On the other hand, the anisotropy shows a nontrivial behavior: although the system is spatially anisotropic due to the photoinduced current, the excited current quickly damps compared to the superconducting fluctuation. Hence we find an isotropic but still nonequilibrium state, which is confirmed through the properties of probe currents. We also perform a systematic study on the parameter dependences on the pump and probe electric currents in all dimensions.

This paper is organized as follows. Section II provides the theoretical formalism for the pump-probe procedure based on the TDGL approach. The numerical results are given in Secs. III and IV, where different pump procedures are taken. We summarize these results in Sec. V. Appendixes A and B are devoted to a detailed explanation for our numerical calculation, and Appendix C summarizes the equilibrium property realized for $t < 0$ (before the pump) and $t \to \infty$. The additional data for three dimensions and one dimension are also shown in Appendix D.

## II. PUMP-PROBE PROCEDURE IN THE TDGL EQUATION

### A. General formulation

Let us begin with the TDGL equation with a random force [34]

$$\Gamma \frac{\partial}{\partial t} \psi(\boldsymbol{r}, t) = -\frac{\delta \mathcal{F}[\psi, \boldsymbol{A}]}{\delta \psi^*(\boldsymbol{r}, t)} + f(\boldsymbol{r}, t), \quad (1)$$

$$\mathcal{F}[\psi, \boldsymbol{A}] = \int d\boldsymbol{r}\, \psi^*(\boldsymbol{r}, t) \left( a - \frac{[\nabla - 2ie\boldsymbol{A}(\boldsymbol{r}, t)]^2}{4m} \right) \psi(\boldsymbol{r}, t), \quad (2)$$

$$\boldsymbol{j}(\boldsymbol{r}, t) = -\frac{\delta \mathcal{F}[\psi, \boldsymbol{A}]}{\delta \boldsymbol{A}(\boldsymbol{r}, t)}, \quad (3)$$

where $\mathcal{F}$ and $\boldsymbol{j}$ are the GL free energy and superconducting current density, respectively, and $\Gamma$ is a time development factor. We have taken $\hbar = k_B = 1$ unless otherwise stated explicitly. The classical complex field $\psi(\boldsymbol{r}, t)$ is the superconducting order parameter or macroscopic wave function. We consider the spatially uniform electric field, and the vector potential can be chosen as the one dependent only on time: $\boldsymbol{A}(\boldsymbol{r}, t) = \boldsymbol{A}(t)$. We note that the fourth-order term $|\psi(\boldsymbol{r}, t)|^4$ is irrelevant here, since we consider the system above the transition temperature ($T > T_c$). The photoexcitations in the superconducting state below $T_c$ have been discussed in Ref. [27]. The coefficient of the second-order term behaves as $a = a'(T - T_c)\,(>0)$ with a constant $a' \sim \frac{k_B^2 T_c}{\varepsilon_F}$ ($\varepsilon_F$ is the Fermi energy).

The random force $f(\boldsymbol{r}, t)$ is also introduced to represent thermal fluctuation. Performing the Fourier transformation,

we get

$$\Gamma \frac{\partial}{\partial t} \psi_{\boldsymbol{q}}(t) = -\left( \frac{[\boldsymbol{q} - 2e\boldsymbol{A}(t)]^2}{4m} + a \right) \psi_{\boldsymbol{q}}(t) + f_{\boldsymbol{q}}(t). \quad (4)$$

The solution for the macroscopic wave function is then written as

$$\psi_{\boldsymbol{q}}(t) = \int_{-\infty}^{t} \frac{dt'}{\Gamma} f_{\boldsymbol{q}}(t')$$
$$\times \exp\left[ -\int_{t'}^{t} \frac{dt''}{\Gamma} \left( \frac{[\boldsymbol{q} - 2e\boldsymbol{A}(t'')]^2}{4m} + a \right) \right]. \quad (5)$$

We assume that $f_{\boldsymbol{q}}(t)$ is spatially and temporally uncorrelated such that the random average (denoted by a bracket symbol) is given by

$$\langle f_{\boldsymbol{q}}^*(t) f_{\boldsymbol{q}'}(t') \rangle = \frac{C}{V} \delta_{\boldsymbol{q}\boldsymbol{q}'} \delta(t - t'), \quad (6)$$

where $V$ is a system volume. The constant $C$ is determined so that the random average is identical to the thermal average [34], which results in $C = 2\Gamma V T$.

The most fundamental physical quantity in our system is the superconducting fluctuation $\langle |\psi|^2 \rangle$. With the random force, the effect of the superconducting fluctuation can be taken into account and the quantity $\langle |\psi_{\boldsymbol{q}}(t)|^2 \rangle$ becomes finite. Since the quantity with the wave vector $\boldsymbol{q}$ is gauge-dependent, we consider the real-space quantity

$$\langle |\psi(\boldsymbol{r}, t)|^2 \rangle = \frac{1}{V} \sum_{\boldsymbol{q}} \langle |\psi_{\boldsymbol{q}}(t)|^2 \rangle, \quad (7)$$

which is now a gauge-invariant quantity, and is also spatially uniform in our present setup. In the analysis, we separate the contributions from the equilibrium state and the nonequilibrium one, and we define the deviation by

$$\delta \langle |\psi_{\boldsymbol{q}}(t)|^2 \rangle = \langle |\psi_{\boldsymbol{q}}(t)|^2 \rangle - \langle |\psi_{\boldsymbol{q}}(t)|^2 \rangle_{\text{eq}}, \quad (8)$$

where $\langle \cdots \rangle_{\text{eq}}$ stands for the equilibrium value. In the following, we use $\delta O$ as the deviation of the quantity $O$ from that in the equilibrium state.

We separate the vector potential into two parts as $\boldsymbol{A} = \boldsymbol{A}_0 + \boldsymbol{A}_1$, where $\boldsymbol{A}_0$ and $\boldsymbol{A}_1$ represent pump and probe lights, respectively. The vector potential $\boldsymbol{A}_1$ for the probe is treated by the linear-response theory. The fluctuation contribution to the electric current density is given by

$$\boldsymbol{j}(t) = \sum_{\boldsymbol{q}} \frac{e}{mV} [\boldsymbol{q} - 2e\boldsymbol{A}(t)] \langle |\psi_{\boldsymbol{q}}(t)|^2 \rangle = \boldsymbol{j}_0(t) + \boldsymbol{j}_1(t), \quad (9)$$

where

$$\boldsymbol{j}_0(t) = \frac{e}{mV} \sum_{\boldsymbol{q}} [\boldsymbol{q} - 2e\boldsymbol{A}_0(t)] \langle |\psi_{\boldsymbol{q}}(t)|^2 \rangle_0, \quad (10)$$

$$\boldsymbol{j}_1(t) = \frac{e}{mV} \sum_{\boldsymbol{q}} [\boldsymbol{q} - 2e\boldsymbol{A}_0(t)] \langle |\psi_{\boldsymbol{q}}(t)|^2 \rangle_1$$
$$- \frac{2e^2}{mV} \sum_{\boldsymbol{q}} \langle |\psi_{\boldsymbol{q}}(t)|^2 \rangle_0 \boldsymbol{A}_1(t). \quad (11)$$

Here $j_0$ is a photoexcited current density and $j_1$ is a small current induced by the probe light. The subscripts 0 and 1 represent the perturbation order of $A_1$. If we consider the equilibrium case, we reproduce the standard paraconductivity formula [29,34], which is summarized in Appendix C based on our formalism. The expressions in Eqs. (10) and (11) can be used in all dimensions. For a film-shaped sample with thickness $d$, the system can be regarded as two-dimensional if the coherence length is much larger than the thickness ($\xi \gg d$). In this case, the measurable three-dimensional current density is given by $j = j_{2D}/d$, where $j_{2D}$ is the current density in two dimensions. In a similar manner, for a wire-shaped sample with cross-sectional area $S = d_x d_y$, the current density is given by $j = j_{1D}/S$ for $\xi \gg d_{x,y}$.

We can also consider the time-dependent GL free energy $\mathcal{F}$, which is modified from the equilibrium by the photoexcitation. After taking the random average, we get

$$\langle \mathcal{F}(\boldsymbol{r}, t) \rangle = \sum_{\boldsymbol{q}} \left( a + \frac{[\boldsymbol{q} - 2e\boldsymbol{A}(t)]^2}{4m} \right) \langle |\psi_{\boldsymbol{q}}(t)|^2 \rangle \quad (12)$$

$$\equiv \mathcal{F}_{\text{fluct}}(t) + \mathcal{F}_{\text{kin}}(t). \quad (13)$$

The first term $\mathcal{F}_{\text{fluct}}(t) = Va\langle |\psi(\boldsymbol{r}, t)|^2 \rangle$ represents the fluctuation contribution to the free energy, and the second term represents the kinetic energy of Cooper pairs. To consider the anisotropy in the kinetic energy, we divide the free energy as $\mathcal{F}_{\text{kin}} = \sum_{\mu} \mathcal{F}_{\text{kin}}^{(\mu)}$, where

$$\mathcal{F}_{\text{kin}}^{(\mu)}(t) = \sum_{\boldsymbol{q}} \frac{[q_\mu - 2eA_\mu(t)]^2}{4m} \langle |\psi_{\boldsymbol{q}}(t)|^2 \rangle. \quad (14)$$

In the next two subsections, we specify the shape of the pump/probe lights more concretely, and we derive the detailed expressions for the above physical quantities.

Here we comment on the validity of the TDGL equation in Eq. (1). As is clear from its expression, the higher-order derivatives in space-time are neglected in Eq. (1), which cannot be justified for a fast excitation process in general. Hence our results at short time after the pump should be regarded as the extrapolation from the slow dynamics. We have also neglected the higher-order terms with respect to the order parameter $\psi$, which can be important when the photoexcitation makes $|\psi|$ larger. However, as shown in the rest of this paper, the amplitude of $\psi$ decreases in general after the pump, and therefore the higher-order term is not necessary in our situation. We note that the higher-order terms such as $|\psi|^4$ must be included for $T < T_c$, although we concentrate here on the $T > T_c$ case.

### B. Single pump-shot model

As the simplest form of the pump process, we consider the electric field with a single delta function [single pump-shot model; see Figs. 1(a) and 1(b)]. The time dependence of the vector potential is

$$\boldsymbol{A}(t) = \boldsymbol{A}_0 \theta(t) + \boldsymbol{A}_1 \theta(t - t_1) \sin \Omega(t - t_1), \quad (15)$$

where $\theta(t)$ is Heaviside's step function. While the realistic setup in the experiments involves an oscillating Gaussian shape, our choice of electric fields makes the equations simple enough to evaluate decaying properties precisely in numerical calculations. More specifically, the integration with respect to time is evaluated analytically, and hence we can focus on the implementation of $\boldsymbol{q}$-integrals. With this setup, the superconducting fluctuation is explicitly written as

$$\delta\langle |\psi_{\boldsymbol{q}}(t)|^2 \rangle = \frac{C}{V\Gamma^2 g(\boldsymbol{q})^{-1}} e^{-tg(\boldsymbol{q}-2e\boldsymbol{A}_0)^{-1}} \left( 1 - \frac{2e(\boldsymbol{q} - 2e\boldsymbol{A}_0) \cdot \boldsymbol{A}_1 \theta(t - t_1)}{m\Gamma\Omega} [\cos \Omega(t - t_1) - 1] \right)$$

$$- \frac{C}{V\Gamma^2 g(\boldsymbol{q}-2e\boldsymbol{A}_0)^{-1}} e^{-tg(\boldsymbol{q}-2e\boldsymbol{A}_0)^{-1}} \left( 1 - \frac{2e(\boldsymbol{q} - 2e\boldsymbol{A}_0) \cdot \boldsymbol{A}_1 \theta(t - t_1)}{m\Gamma\Omega} [\cos \Omega(t - t_1) - 1] \right)$$

$$- \frac{C}{V\Gamma^2} \cdot \frac{2e(\boldsymbol{q} - 2e\boldsymbol{A}_0) \cdot \boldsymbol{A}_1 \theta(t - t_1)}{m\Gamma\Omega} \cdot \frac{g(\boldsymbol{q}-2e\boldsymbol{A}_0)^{-1}}{g(\boldsymbol{q}-2e\boldsymbol{A}_0)^{-2} + \Omega^2} e^{-(t-t_1)g(\boldsymbol{q}-2e\boldsymbol{A}_0)^{-1}} + O(\boldsymbol{A}_1^2), \quad (16)$$

$$\langle |\psi_{\boldsymbol{q}}(t)|^2 \rangle_{\text{eq}} = \frac{C}{V\Gamma^2 g(\boldsymbol{q}-2e\boldsymbol{A}_0)^{-1}} \left( 1 - \frac{2e(\boldsymbol{q} - 2e\boldsymbol{A}_0) \cdot \boldsymbol{A}_1 \theta(t - t_1)}{m\Gamma\Omega} \cos \Omega(t - t_1) \right) + \frac{C}{V\Gamma^2} \cdot \frac{2e(\boldsymbol{q} - 2e\boldsymbol{A}_0) \cdot \boldsymbol{A}_1 \theta(t - t_1)}{m\Gamma\Omega}$$

$$\times \left[ \frac{g(\boldsymbol{q}-2e\boldsymbol{A}_0)^{-1}}{g(\boldsymbol{q}-2e\boldsymbol{A}_0)^{-2} + \Omega^2} \cos \Omega(t - t_1) + \frac{\Omega}{g(\boldsymbol{q}-2e\boldsymbol{A}_0)^{-2} + \Omega^2} \sin \Omega(t - t_1) \right] + \mathcal{O}(\boldsymbol{A}_1^2) \quad (17)$$

for $t > 0$. We have defined the $\boldsymbol{q}$-dependent function by $g(\boldsymbol{q}) = \frac{\Gamma}{2}(\frac{q^2}{4m} + a)^{-1}$ to make the notation simple. There is no exponentially time-dependent factor in $\langle |\psi_{\boldsymbol{q}}(t)|^2 \rangle_{\text{eq}}$, and hence it represents the contribution from equilibrium in the limit $t \to \infty$. Taking the $\boldsymbol{q}$-summations with some form factors, we can get physical quantities such as the order parameter and electric current, which are all gauge-invariant quantities. We note that even after the pump process finishes, there remains a finite vector potential as shown in Fig. 1(a). However, this is not a physical degree of freedom, and it can be eliminated by a constant shift in $\boldsymbol{q}$-summation. We also note that the expression includes exponential functions and the integration range should be carefully chosen in the numerical calculation. The technical details are summarized in Appendixes A and B. With these techniques, we can have highly accurate numerical results that enable us to access the critical exponents of the decaying functions as shown later in Sec. III.
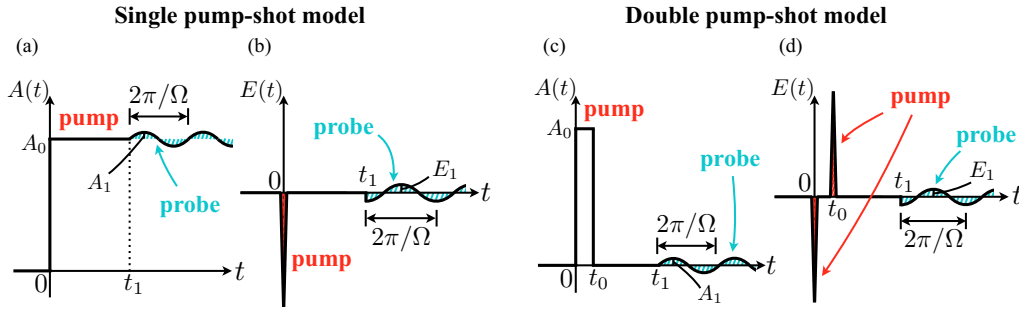
FIG. 1. Sketches for the time dependences of (a) the vector potential and (b) the electric field in the pump-probe process considered in the single pump-shot model. (c), (d) The same plots for the double pump-shot model.

Although in general it is hard to derive the analytical expression, it is possible if we focus on the large $t$ limit. In this case the $q$-integrals are reduced to simple Gaussian integrals, and the superconducting fluctuation, electric current density, and kinetic component of the GL free energy are explicitly obtained as

$$\delta \langle |\psi(\boldsymbol{r}, t)|^2 \rangle \xrightarrow{t \to \infty} \frac{C}{2\Gamma V} \left( \frac{m\Gamma}{2\pi} \right)^{d/2} \left( \frac{m}{e^2 A_0^2 + ma} - \frac{1}{a} \right) t^{-d/2} e^{-\frac{2a}{\Gamma} t}, \tag{18}$$

$$\boldsymbol{j}_0(t) \xrightarrow{t \to \infty} -\frac{C e^2 \boldsymbol{A}_0}{\Gamma V} \left( \frac{m\Gamma}{2\pi} \right)^{d/2} \frac{1}{e^2 A_0^2 + ma} t^{-d/2} e^{-\frac{2a}{\Gamma} t}, \tag{19}$$

$$\delta \mathcal{F}_{\text{kin}}(t) \xrightarrow{t \to \infty} \frac{dC}{8} \left( \frac{m\Gamma}{2\pi} \right)^{d/2} \left( \frac{m}{e^2 A_0^2 + ma} - \frac{1}{a} \right) t^{-\frac{d+2}{2}} e^{-\frac{2a}{\Gamma} t} \tag{20}$$

for the $d$-dimensional system. Namely, the time constant $\Gamma/2a$ [which is identical to $\gamma_1^{-1}$ defined below in Eq. (23)], which originates from the temperature measured from the transition point, gives a characteristic timescale when approaching the equilibrium state. However, the richer behaviors can be seen at a shorter time range, as discussed in Sec. III.

In the above formalism, we have considered the probing light induced at $t = t_1$. In the numerical analysis in Sec. III, however, we focus on the pump light effect for the single pump-shot model. The effects from probing light are considered only for the double pump-shot model (see below), since the setup is the more realistic situation compared to the single pump-shot model.

### C. Double pump-shot model

Here we consider a slightly more realistic situation. Since the electric field is applied with an oscillating manner in the experimental setup, it is natural if the sum rule $\int_0^{t_0} \boldsymbol{E}(t) dt = \boldsymbol{0}$ is satisfied. With this constraint, the simplest form of the electric field is the combination of the two delta functions with different signs [see Figs. 1(c) and 1(d)]. The time dependence of the vector potential is given by

$$\boldsymbol{A}(t) = \boldsymbol{A}_0 \theta(t) \theta(t_0 - t) + \boldsymbol{A}_1 \theta(t - t_1) \sin \Omega(t - t_1). \tag{21}$$

Namely, the pump process appears for $0 < t < t_0$ and the probe process for $t_1 < t$. In this case, the deviation of the superconducting fluctuation from the equilibrium state for $t > t_0$ is written as

$$\delta \langle |\psi_{\boldsymbol{q}}(t)|^2 \rangle = \frac{C}{V \Gamma^2 g(\boldsymbol{q})^{-1}} e^{-(t-t_0)g(\boldsymbol{q})^{-1} - t_0 g(\boldsymbol{q} - 2e\boldsymbol{A}_0)^{-1}} \left( 1 - \frac{2e\boldsymbol{q} \cdot \boldsymbol{A}_1 \theta(t - t_1)}{m\Gamma\Omega} [\cos \Omega(t - t_1) - 1] \right)$$

$$+ \frac{C}{V \Gamma^2 g(\boldsymbol{q} - 2e\boldsymbol{A}_0)^{-1}} [1 - e^{-t_0 g(\boldsymbol{q} - 2e\boldsymbol{A}_0)^{-1}}] e^{-(t-t_0)g(\boldsymbol{q})^{-1}} \left( 1 - \frac{2e\boldsymbol{q} \cdot \boldsymbol{A}_1 \theta(t - t_1)}{m\Gamma\Omega} [\cos \Omega(t - t_1) - 1] \right)$$

$$+ \frac{C}{V \Gamma^2 g(\boldsymbol{q})^{-1}} [e^{-(t-t_1)g(\boldsymbol{q})^{-1}} - e^{-(t-t_0)g(\boldsymbol{q})^{-1}}] \left( 1 - \frac{2e\boldsymbol{q} \cdot \boldsymbol{A}_1 \theta(t - t_1)}{m\Gamma\Omega} [\cos \Omega(t - t_1) - 1] \right)$$

$$- \frac{C}{V \Gamma^2 g(\boldsymbol{q})^{-1}} e^{-(t-t_1)g(\boldsymbol{q})^{-1}} \left( 1 - \frac{2e\boldsymbol{q} \cdot \boldsymbol{A}_1 \theta(t - t_1)}{m\Gamma\Omega} \cos \Omega(t - t_1) \right) - \frac{C}{V \Gamma^2} \cdot \frac{2e\boldsymbol{q} \cdot \boldsymbol{A}_1 \theta(t - t_1)}{m\Gamma\Omega} \cdot \frac{e^{-(t-t_1)g(\boldsymbol{q})^{-1}} g(\boldsymbol{q})^{-1}}{g(\boldsymbol{q})^{-2} + \Omega^2}, \tag{22}$$

where we have kept the terms up to $O(\boldsymbol{A}_1)$ contributions. The order parameter in the equilibrium state is the same as Eq. (17) with the replacement $\boldsymbol{q} - 2e\boldsymbol{A}_0 \to \boldsymbol{q}$. For the time range $0 < t < t_0$, the system is essentially the same as the single pump-shot model, and new expressions are not necessary.
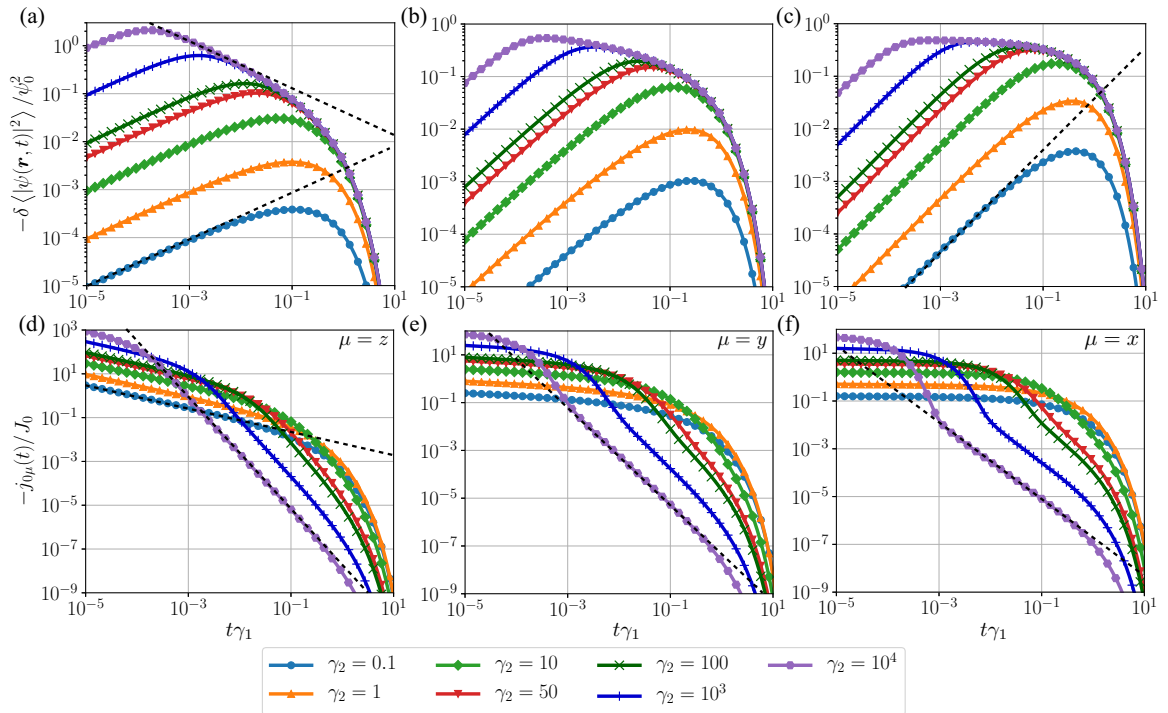
FIG. 2. Time evolution of the (a)–(c) superconducting fluctuation and the (d)–(f) excited current density in the single pump-shot model with a logarithmic scale, which are measured as deviations from the equilibrium component. The quantities are plotted for (a), (d) three-, (b), (e) two-, and (c), (f) one-dimensional systems. The dashed lines shown in (a), (c)–(f) are power functions shown in Eqs. (25)–(28). $\mu$ is the direction where the pump pulse is shot, $\mu = z$ in the (d) three-, $\mu = y$ in the (e) two-, and $\mu = x$ in the (f) one-dimensional system. The normalized constants are defined by $\psi_0^2 = \frac{C}{\gamma_1 \Gamma^2 V} (2m\gamma_1 \Gamma)^{d/2}$ and $J_0 = \frac{eC}{m\gamma_1 \Gamma^2 V} (2m\gamma_1 \Gamma)^{\frac{d+1}{2}}$.

## III. NUMERICAL RESULTS FOR SINGLE PUMP-SHOT MODEL

Here we show the physical quantities in the photoexcited states of the single-pump shot model formulated in Sec. II B. We concentrate on the photoexcited states in this section, and the properties of the probing process are discussed in the more realistic double-pump shot model in the next section. For the single-pump shot model, the behaviors are controlled by the following two parameters:

$$\gamma_1 = \frac{2a}{\Gamma}, \tag{23}$$

$$\gamma_2 = \frac{2e^2 A_0^2}{m\Gamma}, \tag{24}$$

which have the dimension of the inverse of time. $\gamma_1$ represents the distance from the critical point, and $\gamma_2$ shows the intensity of the pump light. We take $\gamma_1 = 1$ as a unit of energy, and the controlling parameter is then $\gamma_2$.

First, we consider the deviation $\delta\langle|\psi(\boldsymbol{r}, t)|^2\rangle$ of the superconducting fluctuation from equilibrium defined in Eq. (16), which is shown in Figs. 2(a)–2(c). These figures are plotted with a logarithmic scale to visualize the functional form of the decaying functions of the physical quantities. After the pump at $t = 0$, the superconducting fluctuation decreases from the equilibrium value, i.e., $\delta\langle|\psi(\boldsymbol{r}, t)|^2\rangle < 0$. The decrease stops at $t \sim \gamma_2^{-1}$, where the fluctuation becomes minimum, and then it increases toward the equilibrium value. It is notable that in the whole time range, the photoexcitation gives a negative

contribution to the superconducting fluctuation, which is in contrast to a naive expectation that the photoexcitation may increase the superconducting fluctuation. The photoinduced electric current is also shown in Figs. 2(d)–2(f), which is a decreasing function with respect to time. Namely, the effect of photoexcitation appears maximally around $t = 0$, which is different from the behaviors of the fluctuation shown in Figs. 2(a)–2(c).

For a sufficiently long time regime, all the quantities in Fig. 2 decay with an exponential form with the damping constant $\gamma_1 (= 1)$. Indeed, this behavior is consistent with the analytical asymptotic form given in Eqs. (18) and (19). In the shorter time regime, on the other hand, we find the power-law or logarithmic behaviors for both the superconducting fluctuation and electric current in all dimensions. Usually the power-law behaviors are observed in systems located at the critical point [38]. In contrast, the present case is away from the transition point ($T > T_c$), but we still observe the power-law decay. In large $\gamma_2$ cases, such as $\gamma_2 = 50$, 100, $10^3$, and $10^4$, the power-law regime is separated into two parts at $t \sim \gamma_2^{-1}$. We can see from Fig. 2 that if we take $\gamma_2 < \gamma_1$, one of the power-law or logarithmic regimes vanishes. In the former studies in nonequilibrium states, the power-law behavior in superconductors has also been found in Refs. [39] and [40].

The above exponential and power-law/logarithmic behaviors are summarized in Fig. 3, which is one of the central results of this paper. The phase diagram in the plane of $t$ and $\gamma_2$ is categorized into three regimes: the exponentially decaying regime ($t > \gamma_1^{-1}$, III), the power-law or logarithmic decaying
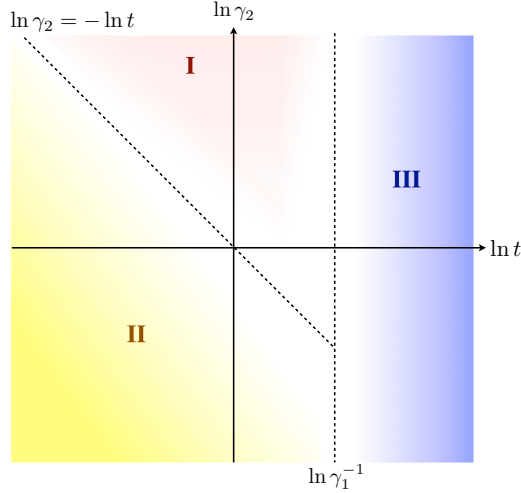
FIG. 3. A sketch of the phase diagram in the plane of the logarithmic time $\ln t$ and the logarithmic excitation strength $\ln \gamma_2$. The dashed lines show crossovers.

regime ($\gamma_2^{-1} < t < \gamma_1^{-1}$, I), and another power-law regime ($t < \gamma_2^{-1}$, II). The pump-pulse intensity $\gamma_2$ characterizes the power-law/logarithmic damping behavior, while the system temperature $\gamma_1 \propto (T - T_c)$ characterizes exponentially decaying behavior. The line that separates regimes I and II terminates at the point where it crosses with the vertical $t = \gamma_1^{-1}$ line.

The power-law/logarithmic behavior is intuitively interpreted as follows. When the system is very close to the superconducting transition point, the value of $\gamma_1^{-1} \sim a^{-1}$ goes to infinity and then only regimes I and II are left. Hence this power-law/logarithmic decay originates from a characteristic behavior at the critical point. For a sufficiently weak pump, regime II survives for a long time, whereas regime I is dominant for a strong pump with large $\gamma_2 \propto A_0^2$. Away from the critical point ($a > 0$), the power-law/logarithmic regimes end at the time scale of $\gamma_1^{-1}$ and crossover into the exponentially decaying regime. This indicates that the critical point is effectively expanded into a finite regime by the pump shot and it shrinks with evolving time to approach the equilibrium state. We note that the fluctuation itself is suppressed, as shown in Figs. 2(a) and 2(c) and Eq. (16), although it is divergent at the critical point in equilibrium. Hence the behavior with the power-law/logarithmic decay and with finite fluctuation amplitude is characteristic for an excited state in nonequilibrium.

We also comment on the region in which the GL approach is justified. The GL theory can account for the long wavelength and slow dynamics, and the corresponding characteristic length and time are given by the coherence length $\xi \sim \hbar/\sqrt{ma}$ and the correlation time $t_c \sim \Gamma/a \sim \gamma_1^{-1}$. Hence the time range with $t \ll t_c \sim \gamma_1^{-1}$ is not justified in a strict sense, but rather our results should be regarded as an extrapolation from the GL theory.

With the help of Fig. 3, we can have analytic forms of the power-law and logarithmic functions. For regime I

($\gamma_2^{-1} < t < \gamma_1^{-1}$), we take the limit $\gamma_2 \to \infty$ and obtain the asymptotic behaviors of fluctuations and currents for each dimension as

$$\delta\langle|\psi(\mathbf{r},t)|^2\rangle \simeq \begin{cases} -\dfrac{4\pi mC}{V}\sqrt{\dfrac{2\pi m}{\Gamma}}\, t^{-1/2} & (d=3), \\[2ex] \dfrac{2\pi mC}{\Gamma V}\left[\gamma + \ln\left(\dfrac{2a}{\Gamma}t\right)\right] & (d=2), \\[2ex] -\dfrac{\pi C}{\Gamma V}\sqrt{\dfrac{m}{a}} & (d=1), \end{cases} \quad (25)$$

$$\mathbf{j}_0(t) \simeq \begin{cases} -\dfrac{2\pi m^2 \Gamma C A_0}{Ve^2 A_0^4}\sqrt{\dfrac{\pi m\Gamma}{2}}\, t^{-5/2} & (d=3), \\[2ex] -\dfrac{\pi m^2 C A_0}{Ve^2 A_0^4}\, t^{-2} & (d=2), \\[2ex] -\dfrac{mCA_0}{Ve^2 A_0^4}\sqrt{\dfrac{\pi m\Gamma}{2}}\, t^{-3/2} & (d=1), \end{cases} \quad (26)$$

where $\gamma$ is Euler's gamma constant. For regime II ($t < \gamma_2^{-1}$), on the other hand, the critical behaviors are seen in the weak excitation limit ($\gamma_2 \to 0$). We then obtain the time dependences as

$$\delta\langle|\psi(\mathbf{r},t)|^2\rangle \simeq \begin{cases} -\dfrac{2e^2 A_0^2 C}{3\pi \Gamma^2 V}\sqrt{\dfrac{2m}{\pi \Gamma}}\, t^{1/2} & (d=3), \\[2ex] \dfrac{e^2 A_0^2 C}{\pi \Gamma^2 V}\, t\left[\gamma + \ln\left(\dfrac{2a}{\Gamma}t\right)\right] & (d=2), \\[2ex] -\dfrac{e^2 A_0^2 C}{m\Gamma^2 V}\sqrt{\dfrac{m}{a}}\, t & (d=1), \end{cases}$$
$$(27)$$

$$\mathbf{j}_0(t) \simeq \begin{cases} -\dfrac{16\pi Ce^2 A_0}{3V}\sqrt{\dfrac{2\pi m}{\Gamma}}\, t^{-1/2} & (d=3), \\[2ex] \dfrac{4\pi Ce^2 A_0}{\Gamma V}\left[\gamma + \ln\left(\dfrac{2a}{\Gamma}t\right)\right] & (d=2), \\[2ex] -\dfrac{2\pi Ce^2 A_0}{V}\sqrt{\dfrac{2}{ma}} & (d=1). \end{cases} \quad (28)$$

These time dependences are consistent with the numerical results shown in Fig. 2.

Let us turn our attention to the photoexcitation effects on the free energy. Figures 4(a)–4(c) show the time dependence of the total GL free energy $\delta\mathcal{F}(t)$ defined in Eq. (12) for the fixed $A_0$. The total free energy $\delta\mathcal{F}(t)$ increases substantially after the pump, whose main contribution comes from the kinetic energy. We also plot the direction-dependent kinetic energy $\delta\mathcal{F}_{\text{kin}}^{(\mu)}$ defined in Eq. (14) and the fluctuation contribution $\delta\mathcal{F}_{\text{fluct}}$. For the three-dimensional case shown in Fig. 4(a), the kinetic energy along the $z$ direction is positive, while the other $x$, $y$-direction components are negative. With evolving time, the kinetic energy decreases and the nonequilibrium component of the total free energy becomes negative. This sign change is captured by analytic asymptotic functions for
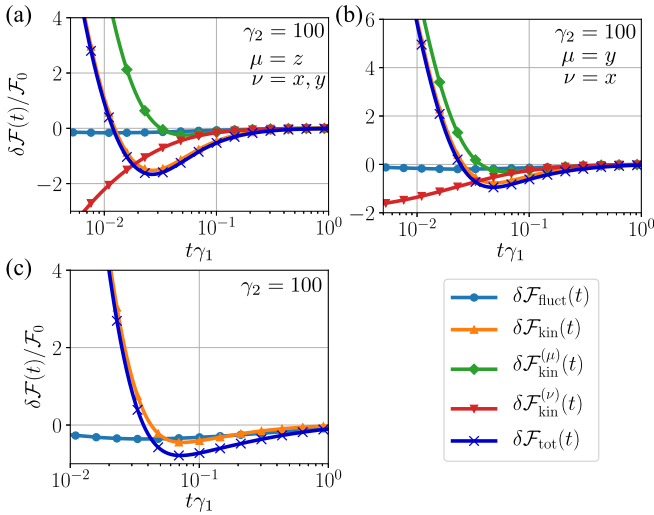
FIG. 4. Time dependence of the GL free energy defined in Eq. (12) in the single pump-shot model ($\delta\mathcal{F}_{\text{tot}} = \delta\mathcal{F}_{\text{fluct}} + \delta\mathcal{F}_{\text{kin}}$) in the (a) three-, (b) two-, and (c) one-dimensional systems, and we have taken $\gamma_2 = 100$. $\mu$ and $\nu$ mean the components of the kinetic GL free energy, where $\mu$ is the direction where the pump pulse is shot and $\nu$ is the other direction, $\mu = z$, and $\nu = x, y$ in the (a) three-dimensional system and $\mu = y$ and $\nu = x$ in the (b) two-dimensional system. The normalized constant is defined by $\mathcal{F}_0 = \frac{C}{2\Gamma}(2m\gamma_1\Gamma)^{d/2}$.

the kinetic energy, whose forms are

$$
\delta\mathcal{F}_{\text{kin}}(t) \sim
\begin{cases}
-\dfrac{mC}{4\pi}\sqrt{\dfrac{m\Gamma}{2\pi}}\, t^{-3/2} & (d = 3), \\[2ex]
-\dfrac{mC}{4\pi}\, t^{-1} & (d = 2), \\[2ex]
-\dfrac{C}{2\Gamma}\sqrt{\dfrac{m\Gamma}{2\pi}}\, t^{-1/2} & (d = 1)
\end{cases}
\tag{29}
$$

for $\gamma_2^{-1} < t < \gamma_1^{-1}$ (regime I), and

$$
\delta\mathcal{F}_{\text{kin}}(t) \sim
\begin{cases}
\dfrac{e^2 A_0^2 C}{6\pi\,\Gamma}\sqrt{\dfrac{2m\Gamma}{\pi}}\, t^{-1/2} & (d = 3), \\[2ex]
-\dfrac{e^2 A_0^2 C}{2\pi}\left[\gamma + \ln\left(\dfrac{2a}{\Gamma}t\right)\right] & (d = 2), \\[2ex]
\dfrac{e^2 A_0^2 C}{2m\Gamma}\sqrt{\dfrac{m}{a}} & (d = 1)
\end{cases}
\tag{30}
$$

for $t < \gamma_2^{-1}$ (regime II). The fluctuation contribution $\delta\mathcal{F}_{\text{fluct}}(t)$ is basically the same quantity as the superconducting fluctuation given by $\delta\langle|\psi(\mathbf{r}, t)|^2\rangle$. In Fig. 4, however, it does not make a significant contribution to the free energy.

At the end of this section, let us estimate the realistic values for the characteristic timescales and observable current signals. We focus on the two-dimensional system as in the cuprate superconductors where the fluctuation phenomena have been observed. We first consider the time constants $\gamma_1^{-1}, \gamma_2^{-1}$ defined in Eqs. (23) and (24). For the estimation, we employ the results from the BCS theory, $a \sim \frac{(k_B T_c)^2}{\varepsilon_F}\frac{T-T_c}{T_c}$ and $\Gamma \sim \frac{k_B T_c}{\varepsilon_F}\hbar$ [32]. Taking $\varepsilon_F = 1.0$ eV, $T_c = 1.0 \times 10^2$ K, and $T = 1.1T_c$, we obtain $\gamma_1^{-1} \simeq 1.5 \times 10^{-1}$ ps. As for the

estimation of $\gamma_2^{-1}$, we need the value of the strength of the electric field $E_0$ and its duration time $\tau$. Although we consider the delta function for the pump electric field in Fig. 1, we regard it as a box shape with the width $\tau$ and the height $E_0\tau$. For a typical experimental situation, the strength of the electric field is roughly $E_0 \sim 1$ MV/cm and the duration is $\tau \sim 1$ ps [11]. With these conditions we get $\gamma_2^{-1} \sim 1.6 \times 10^{-10}$ ps, which is much smaller than $\gamma_1^{-1}$. Hence, region I in Fig. 3 is likely to be observed.

We also make an estimate of the value of the photoinduced current. Using the above parameters, we obtain the normalization current density $J_0$, which is defined in the inset of Fig. 2, as $J_0 = 1.5 \times 10^2$ A m$^{-1}$. This value is compared to the normal current, which is simultaneously induced by light. The normal conductivity is typically $\sigma_n \sim 1.0 \times 10^3$ $\Omega^{-1}$ cm$^{-1}$ in the normal state [41]. Using the same $E_0$ as above and the distance 10 Å between the layers made of coppers and oxygens in cuprates, we obtain the normal current density $J_n \sim 10^4$ A m$^{-1}$. Since the signal from fluctuation currents can be 10 or 100 times larger than $J_0$, as shown in Fig. 2, the photoinduced current can be comparable to the normal current in the short time region.

## IV. NUMERICAL RESULTS FOR THE DOUBLE PUMP-SHOT MODEL

We consider the more realistic double pump-shot model shown in Figs. 1(c) and 1(d) as introduced in Sec. II C. We take $t_0 = 1$ as a unit of time, which is located at the end of the pump process [see Figs. 1(c) and 1(d)]. In this section, we discuss only the two-dimensional system because the behaviors are similar in the other dimensions. The results for the one- or three-dimensional system are shown in Appendix D to make the data complete.

### A. Properties of the excited state

We first summarize the results for the excited state here, and then we discuss the probe current in the next subsection. The electric field pulse is induced at $t = 0$ along the $-y$ direction, and at $t = t_0$ along the $+y$ direction for two dimensions. Correspondingly, the physical quantities are largely modified around these two characteristic time scales. Since the results for the time range $0 < t < t_0$ are the same as in the single-shot model, we focus on the regime $t > t_0$. Figure 5(a) shows the time dependence of the superconducting fluctuation in the double pump-shot model. The damping behavior is similar to that in the single pump-shot model: the power-law and exponential decay are observed. At short time, however, there is almost no time dependence. This is due to the remaining nonequilibrium contribution at $t = t_0$ induced from the first pump shot at $t = 0$, which makes the difference from the single pump-shot model. On the other hand, with strong pump, the power-law/logarithmic behavior is observed, which corresponds to regime I in Fig. 3. Namely, while regime II in the single pump-shot model may not be seen depending on the excitation process, regime I is more robustly present for the case with a strong excitation pulse.

Figure 5(b) shows the electric current density. In contrast to Fig. 5(a), the qualitative behaviors are the same as those in the
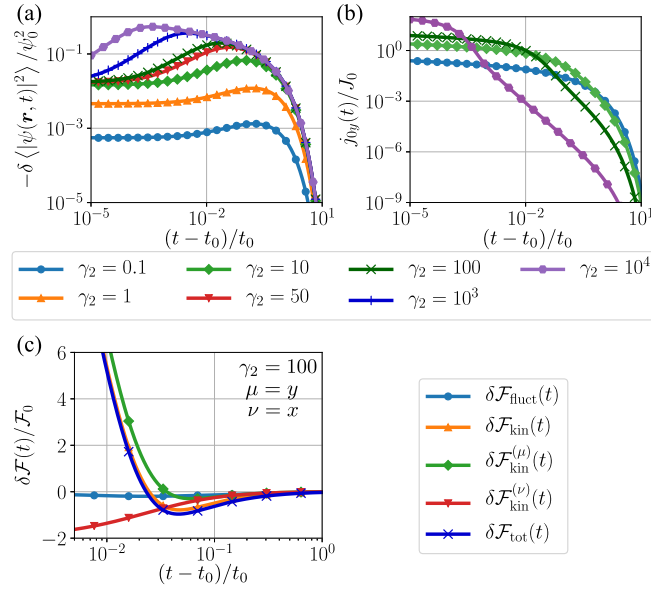
FIG. 5. Time dependences of (a) the superconducting fluctuation, (b) the excited current density, and (c) the GL free energy with the logarithmic time scale in the double pump-shot model. We have taken $t_0 = 1$, $\gamma_1 = 1$, and (c) $\gamma_2 = 100$ to compare with the results of the single pump-shot model in the two-dimensional system. $\mu$ and $\nu$ used in (c) have the same meanings as Fig. 4(b). The normalized constants are defined by $\psi_0^2 = \frac{2mC}{\Gamma V}$, $J_0 = \frac{2eC}{\Gamma V}\sqrt{\frac{2m\Gamma}{t_0}}$, and $\mathcal{F}_0 = \frac{mC}{t_0}$.

single pump-shot model even for small $t - t_0$ [see Fig. 2(e)]. This is because the current induced from the first shot at $t = 0$ is a simple decreasing function and almost vanishes at $t = t_0$, where the second pulse is induced. Thus the characteristic power-law/logarithmic behaviors are not specific to the single pump-shot model. We also show in Fig. 5(c) the time evolution of the free energies, which is again similar to the single pump-shot model. The estimated signal for the double pump-shot model is the same order of magnitude as in the single pump-shot model if the strength of the external field is the same (see also the discussions at the end of Sec. III).

## B. Paraconductivity in photoexcited systems

In this subsection, we consider the probe current in the photoexcited state. With the two-dimensional double pump-shot model, the probe electric field is written as $\boldsymbol{E}_1(t) = \boldsymbol{E}_1 \cos \Omega(t - t_1)$, and the current density in Eq. (11) is written as

$$
\begin{aligned}
j_{1\mu}(t, \Omega) = \sum_\nu \big[ &\sigma_{\mu\nu}^{(1)}(t, \Omega)[\cos \Omega(t - t_1) - 1] \\
&+ \sigma_{\mu\nu}^{(2)}(t, \Omega) \sin \Omega(t - t_1) + \sigma_{\mu\nu}^{(3)}(t, \Omega)\big] E_{1\nu},
\end{aligned}
\tag{31}
$$

where $\mu, \nu = x, y, z$. In equilibrium, if we take the time average, $\sigma^{(1)}$ and $\sigma^{(2)}$ represent the real and imaginary parts of the ac paraconductivity summarized in Appendix C, and $\sigma^{(3)} = 0$.

Let us first focus on the dc paraconductivity with $\Omega \to 0$. In this case, the probe current measured from the equilibrium
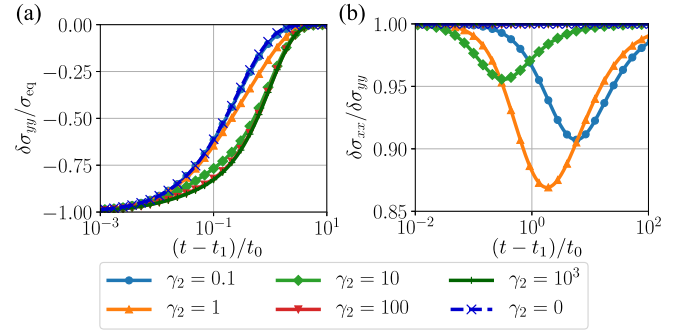


FIG. 6. (a) Time dependence of the nonequilibrium component of the dc paraconductivity, which is normalized by its equilibrium component $\sigma_{\text{eq}} = \frac{e^2 C}{2\pi V a}$. (b) Anisotropy parameter $\delta\sigma_{xx}/\delta\sigma_{yy}$. Note that the vertical axis in (b) is measured from unity (isotropic limit). We have taken $\gamma_1 = 1$ and $t_1 = 1.1$ with the time unit $t_0 (= 1)$.

value is simply written as

$$
\delta j_{1\mu}(t) = \delta\sigma_{\mu\mu}(t) E_{1\mu},
\tag{32}
$$

which describes the characteristics of the nonequilibrium state. Figure 6(a) shows the dc paraconductivity in the photoexcited states for $\gamma_1 = 1$ and $t_1 = 1.1$, which is normalized by the equilibrium component of the conductivity ($\sigma = \sigma_{\text{eq}} + \delta\sigma$). We note that $\delta\sigma_{\mu\mu}(t)$ can be finite even for the case without pump (i.e., $\boldsymbol{A}_0 = \boldsymbol{0}$), since the sudden switching-on of the probing field turns the system into nonequilibrium. As shown in Fig. 6, the paraconductivity is decreased (i.e., $\delta\sigma < 0$) when the pump light $\boldsymbol{A}_0$ is induced. This observation is consistent with the decrease of the superconducting fluctuation in Fig. 5(a). Hence, this result cannot account for the experiments in which the conductivity is largely enhanced [4,13]. A relatively small change in Fig. 6 as a function $\gamma_2$ is due to the choice of measuring time $t_1 = 1.1$: at this time the induced current has become a small value. Since $\delta\sigma$ is the same order of magnitude as the equilibrium component $\sigma_{\text{eq}}$, the paraconductivity characteristic for nonequilibrium states can in principle be observed for the two- and one-dimensional systems where the paraconductivity $\sigma_{\text{eq}}$ is detectable.

With the pump process, the system becomes anisotropic because of the one-direction-oriented electric fields. We show in Fig. 6(b) the anisotropy parameter $\delta\sigma_{xx}/\delta\sigma_{yy}$ for the nonequilibrium component of the paraconductivity. This quantity shows a peaked structure as a function of time. Namely, the photoexcited current makes the system anisotropic and for $t \to \infty$ the system relaxes into the isotropic equilibrium state. The parameter $\gamma_2$-dependence is also not simple. For a weak pump such as $\gamma_2 = 0.1$, the photoinduced current $\boldsymbol{j}_0$ is small and then the anisotropy is also small. With increasing $\gamma_2$, the anisotropy parameter increases with increasing photoinduced current. However, for a sufficiently strong pump, the anisotropy becomes smaller again, as shown in Fig. 6(b). This is because the strong pump creates a quickly damping current with a large exponent, as shown in Eq. (26), and little current is left when probing current is induced. Thus the anisotropy behaves in a nontrivial manner as a function of $\gamma_2$.
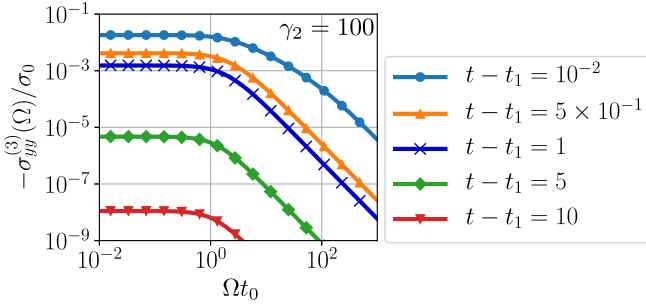
FIG. 7. Frequency dependence of the ac paraconductivity $\sigma^{(3)}$ at several different times. In these figures, we have taken $\gamma_1 = 1$, $\gamma_2 = 100$, and $t_1 = 1.1$ ($t_0 = 1$ is the unit of time). The normalization constant is defined by $\sigma_0 = \frac{8e^2 C t_0}{\Gamma V}$.

Finally, we briefly discuss the ac paraconductivity in the photoexcited state. We can separate the time and frequency dependences of $\delta\sigma^{(1,2)}$, which are written as

$$\delta\sigma_{\mu\mu}^{(1)}(t, \Omega) = \frac{8e^2}{m\Gamma V} \frac{\delta\mathcal{F}_{\text{kin}}^{(\mu)}(t)}{\Omega^2}, \tag{33}$$

$$\delta\sigma_{\mu\mu}^{(2)}(t, \Omega) = \frac{2e^2}{m} \frac{\delta\langle|\psi(\mathbf{r}, t)|^2\rangle}{\Omega}, \tag{34}$$

where $\mu$ means the direction where the pump pulse is shot. These forms can be understood from Eqs. (9), (10), (11), (14), (22), and (31). The time dependence of these quantities has already been discussed in the above, and new plots are not necessary.

The behaviors of $\sigma^{(3)}$ are more complex because we cannot separate the time $t$ and frequency $\Omega$ dependences. Figure 7 shows the frequency dependence of $\sigma^{(3)}(t, \Omega)$ at different times. We can see from Fig. 7 that $\sigma^{(3)}$ is also a simple decreasing function of both time and frequency. Since $\sigma^{(3)}$ behaves as a constant for $\Omega \to 0$ and $\sim\Omega^{-2}$ for the large-$\Omega$ limit, its shape is Lorentzian-like. Thus all the frequency dependences are characterized by the three components $\delta\sigma^{(1,2,3)}(t, \Omega)$.

## V. SUMMARY

Based on the time-dependent Ginzburg-Landau (TDGL) theory, we have clarified the properties of superconducting fluctuation for systems with photoexcitation. While the long-time behavior approaching equilibrium is characterized by exponential decay with a time constant determined by the temperature, in the intermediate regime the nontrivial power-law/logarithmically decaying regimes are identified. The power-law/logarithmic decay is usually observed in systems located at the critical point, but it can be seen in the photoexcited system even away from the critical point, and the exponents are different depending on the excitation strength. This is interpreted as an extension of the critical point into a finite regime by photoexcitation. Although the superconducting fluctuation is divergent at the critical point in the equilibrium case, in the excited state it is reduced from the value in equilibrium for the whole time range.

In addition to the properties of excited states, we have also formulated and calculated the probing currents using the linear-response theory. We have measured the anisotropy of the conductivity in the excited state, which becomes maximal at the intermediate photoexcitation strength, in contrast to a naive expectation that the stronger pump just creates a larger anisotropic state. This behavior is closely related to the exponent change in the current density as a function of the excitation amplitude in the power-law decaying regime. We have also clarified the time evolution of the ac conductivities. The probing currents discussed in this paper may be experimentally observed in one- and two-dimensional systems since the magnitude of the nonequilibrium components of the linear-response conductivity is comparable to the equilibrium one.

These results are obtained based on the simple TDGL equation, which is applicable to a wide class of materials, and it provides a foundation for further exploration of the fluctuation phenomena in nonequilibrium superconductors.

## APPENDIX A: DIMENSIONLESS FORMS OF PHYSICAL QUANTITIES

### 1. Definition of dimensionless functions

In this Appendix, we define dimensionless functions to evaluate the physical quantities numerically. First of all, we introduce the unit time $\mathcal{T}$, which is chosen as $\gamma_1^{-1}$ for the single pump-shot model and as $t_0$ for the double pump-shot model, to make the notation simple. In addition, we define the constants as

$$q_0 = \sqrt{\frac{2m\Gamma}{\mathcal{T}}}, \quad k = \gamma_1 \mathcal{T}, \quad \mathbf{x}_0 = \text{sgn}(e)\sqrt{\gamma_2 \mathcal{T}} \frac{\mathbf{A}_0}{|\mathbf{A}_0|}, \tag{A1}$$

where the definitions of $\gamma_1$ and $\gamma_2$ are given in Eqs. (23) and (24). We have chosen $x_0 > 0$ in this paper. Using these constants, the wave vector is written as $\mathbf{q} - 2e\mathbf{A}_0 = q_0(\mathbf{x} - \mathbf{x}_0)$. We define several dimensionless functions in a $d$-dimensional system as

$$X(a, b) = \int \frac{d\mathbf{x}}{(2\pi)^d} \frac{1}{\mathbf{x}^2 + k} e^{-(a+b)(\mathbf{x} - \frac{b}{a+b}\mathbf{x}_0)^2}, \tag{A2}$$

$$\tilde{X}(a, b) = \int \frac{d\mathbf{x}}{(2\pi)^d} \frac{1}{(\mathbf{x} - \mathbf{x}_0)^2 + k} e^{-(a+b)(\mathbf{x} - \frac{b}{a+b}\mathbf{x}_0)^2}, \tag{A3}$$

$$Y_\mu(a, b) = \int \frac{d\mathbf{x}}{(2\pi)^d} \frac{x_\mu}{\mathbf{x}^2 + k} e^{-(a+b)(\mathbf{x} - \frac{b}{a+b}\mathbf{x}_0)^2}, \tag{A4}$$

$$\tilde{Y}_\mu(a, b) = \int \frac{d\mathbf{x}}{(2\pi)^d} \frac{x_\mu}{(\mathbf{x} - \mathbf{x}_0)^2 + k} e^{-(a+b)(\mathbf{x} - \frac{b}{a+b}\mathbf{x}_0)^2}, \tag{A5}$$

$$Z_{\mu\nu}(a, b) = \int \frac{d\mathbf{x}}{(2\pi)^d} \frac{x_\mu x_\nu}{\mathbf{x}^2 + k} e^{-(a+b)(\mathbf{x} - \frac{b}{a+b}\mathbf{x}_0)^2}, \tag{A6}$$

$$\tilde{Z}_{\mu\nu}(a,b) = \int \frac{d\boldsymbol{x}}{(2\pi)^d} \frac{x_\mu x_\nu}{(\boldsymbol{x}-\boldsymbol{x}_0)^2+k} e^{-(a+b)(\boldsymbol{x}-\frac{b}{a+b}\boldsymbol{x}_0)^2}, \quad (A7)$$

$$W(a,c) = \frac{1}{d} \int \frac{d\boldsymbol{x}}{(2\pi)^d} \frac{\boldsymbol{x}^2(\boldsymbol{x}^2+k)e^{-a\boldsymbol{x}^2}}{(\boldsymbol{x}^2+k)^2+c^2}, \quad (A8)$$

$$\xrightarrow[c\to 0]{} W(a,0) - W^{(2)}(a)c^2 + O(c^4), \quad (A9)$$

$$W^{(2)}(a) = \frac{1}{d} \int \frac{d\boldsymbol{x}}{(2\pi)^d} \frac{\boldsymbol{x}^2 e^{-a\boldsymbol{x}^2}}{(\boldsymbol{x}^2+k)^3}, \quad (A10)$$

$$V(a,c) = -\frac{1}{d} \int \frac{d\boldsymbol{x}}{(2\pi)^d} \frac{\boldsymbol{x}^2 e^{-a\boldsymbol{x}^2}}{(\boldsymbol{x}^2+k)^2[(\boldsymbol{x}^2+k)^2+c^2]}, \quad (A11)$$

which are evaluated for each dimension separately. The limit $c \to 0$ corresponds to the limit $\Omega \to 0$. The function $W^{(2)}$ is used when we consider the dc paraconductivity. We note that $Y_\mu(a,0) = 0$ since the integrand is an odd function, and there is the relation $Z_{\mu\nu}(a,0) = \delta_{\mu\nu} W(a,0)$.

### a. Three-dimensional system

We can choose $\boldsymbol{A}_0 = A_0\hat{\boldsymbol{z}}$ without a loss of generality. Then we have the relations

$$Y_x = Y_y = 0, \quad (A12)$$

$$Z_{\mu\nu} = 0 \ (\mu \neq \nu), \quad (A13)$$

$$Z_{xx} = Z_{yy}, \quad (A14)$$

since the integrand is an odd function. We obtain the detailed functional forms as

$$X(a,b) = \frac{1}{4\pi^2\sqrt{a+b}} G_0\left(k(a+b), \frac{2bx_0}{\sqrt{a+b}}\right), \quad (A15)$$

$$Y_z(a,b) = \frac{1}{4\pi^2(a+b)} G_1\left(k(a+b), \frac{2bx_0}{\sqrt{a+b}}\right), \quad (A16)$$

$$Z_{zz}(a,b) = \frac{1}{4\pi^2(a+b)^{3/2}} G_2\left(k(a+b), \frac{2bx_0}{\sqrt{a+b}}\right), \quad (A17)$$

$$Z_{xx}(a,b) = \frac{\sqrt{\pi}}{16\pi^2(a+b)^{3/2}} - \frac{k}{2}X(a,b) - \frac{1}{2}Z_{zz}(a,b). \quad (A18)$$

Here the function $G_k(a,b)$ is defined by

$$G_k(a,b) = e^{-\frac{b^2}{4}} \int_0^\infty dx \frac{x^{k+2}e^{-x^2}}{x^2+a} \int_{-1}^1 ds\, s^k e^{bxs} \quad (A19)$$

$$= e^{-\frac{b^2}{4}} \sum_{\sigma=\pm} \sum_{l=0}^k \sigma^{l-1} b^{l-k-1} a_l^{(k)} F_{l+1}(a, \sigma b), \quad (A20)$$

where

$$\{a_l^{(0)}\} = 1, \quad (A21)$$

$$\{a_l^{(1)}\} = -1, 1, \quad (A22)$$

$$\{a_l^{(2)}\} = 2, -2, 1, \quad (A23)$$

$$\{a_l^{(3)}\} = -6, 6, -3, 1, \quad (A24)$$

and

$$F_n(a,b) = \int_0^\infty dx \frac{x^n e^{-(x-\frac{b}{2})^2}}{x^2+a}. \quad (A25)$$

### b. Two-dimensional system

We can choose $\boldsymbol{A}_0 = A_0\hat{\boldsymbol{y}}$ without loss of generality. Then, we use the relations

$$Y_x = 0, \quad (A26)$$

$$Z_{\mu\nu} = 0 \ (\mu \neq \nu). \quad (A27)$$

We get

$$X(a,b) = \frac{1}{2\pi} G^{(1)}\left(k(a+b), \frac{2bx_0}{\sqrt{a+b}}\right), \quad (A28)$$

$$Y_y(a,b) = \frac{1}{2\pi\sqrt{a+b}} G^{(2)}\left(k(a+b), \frac{2bx_0}{\sqrt{a+b}}\right), \quad (A29)$$

$$Z_{yy}(a,b) = \frac{1}{4\pi(a+b)} G^{(3)}\left(k(a+b), \frac{2bx_0}{\sqrt{a+b}}\right), \quad (A30)$$

$$Z_{xx}(a,b) = \frac{1}{4\pi(a+b)} G^{(4)}\left(k(a+b), \frac{2bx_0}{\sqrt{a+b}}\right). \quad (A31)$$

We have defined the new functions

$$G^{(1)}(a,b) = \int_0^\infty dx \frac{xe^{-(x-\frac{b}{2})^2}}{x^2+a} \tilde{I}_0(bx), \quad (A32)$$

$$G^{(2)}(a,b) = \int_0^\infty dx \frac{x^2 e^{-(x-\frac{b}{2})^2}}{x^2+a} \tilde{I}_1(bx), \quad (A33)$$

$$G^{(3)}(a,b) = \int_0^\infty dx \frac{x^3 e^{-(x-\frac{b}{2})^2}}{x^2+a} [\tilde{I}_0(bx) + \tilde{I}_2(bx)], \quad (A34)$$

$$G^{(4)}(a,b) = \int_0^\infty dx \frac{x^3 e^{-(x-\frac{b}{2})^2}}{x^2+a} [\tilde{I}_0(bx) - \tilde{I}_2(bx)], \quad (A35)$$

where $\tilde{I}_n(z) = e^{-|z|} I_n(z)$ and $I_n(z)$ is a modified Bessel function of the first kind.

### c. One-dimensional system

We obtain the dimensionless functions in the following forms:

$$X(a,b) = \frac{\sqrt{a+b}}{2\pi} \sum_{s=\pm} F_0\left(k(a+b), \frac{2bx_0 s}{\sqrt{a+b}}\right), \quad (A36)$$

$$Y_x(a,b) = \frac{1}{2\pi} \sum_{s=\pm} sF_1\left(k(a+b), \frac{2bx_0 s}{\sqrt{a+b}}\right), \quad (A37)$$

$$Z_{xx}(a,b) = \frac{1}{2\pi\sqrt{a+b}} \sum_{s=\pm} F_2\left(k(a+b), \frac{2bx_0 s}{\sqrt{a+b}}\right), \quad (A38)$$

where the function $F_n(a,b)$ is given in Eq. (A25).

### 2. Single pump-shot model

We consider the physical quantities in the single pump-shot model. We first define the constants by

$$J_0 = \frac{eC\mathcal{T}q_0^{d+1}}{m\Gamma^2 V}, \tag{A39}$$

$$\sigma_0 = \frac{2e^2 C\mathcal{T}^3 q_0^{d+2}}{m^2\Gamma^3 V}, \tag{A40}$$

$$\psi_0^2 = \frac{C\mathcal{T}q_0^d}{\Gamma^2 V}, \tag{A41}$$

$$\mathcal{F}_0 = \frac{C\mathcal{T}q_0^{d+2}}{4m\Gamma^2}. \tag{A42}$$

The electric current density defined in Eqs. (9), (10), and (11) is rewritten as

$$\delta j_\mu(t,\Omega) = e^{-kt/\mathcal{T}}\left[-J_0\tilde{Y}_\mu\left(\frac{t}{\mathcal{T}},0\right) + \sigma_0\frac{E_{1\mu}^s(t)}{2\Omega\mathcal{T}}X\left(0,\frac{t}{\mathcal{T}}\right) + \sigma_0\sum_\nu\frac{E_{1\nu}^c(t)}{\Omega^2\mathcal{T}^2}\tilde{Z}_{\mu\nu}\left(\frac{t}{\mathcal{T}},0\right)\right]$$
$$- e^{-kt/\mathcal{T}}\left[\sigma_0\frac{E_{1\mu}^s(t)}{2\Omega\mathcal{T}}X\left(\frac{t}{\mathcal{T}},0\right) + \sigma_0\frac{E_{1\mu}^c(t)}{\Omega^2\mathcal{T}^2}W\left(\frac{t}{\mathcal{T}},0\right)\right] + e^{-k(t-t_1)/\mathcal{T}}\sigma_0 E_{1\mu}V\left(\frac{t-t_1}{\mathcal{T}},\Omega\mathcal{T}\right), \tag{A43}$$

where we have defined $\boldsymbol{E}_1^s(t) = \boldsymbol{E}_1\sin\Omega(t-t_1)$ and $\boldsymbol{E}_1^c(t) = \boldsymbol{E}_1[\cos\Omega(t-t_1)-1]$ to make the notations simple. When we take the $\Omega \to 0$ limit, we expand these expressions up to second order.

The deviation of the superconducting fluctuation originating from the pump is given by

$$\frac{\delta\langle|\psi(\boldsymbol{r},t)|^2\rangle}{\psi_0^2} = e^{-kt/\mathcal{T}}X\left(0,\frac{t}{\mathcal{T}}\right) - e^{-kt/\mathcal{T}}\tilde{X}\left(0,\frac{t}{\mathcal{T}}\right). \tag{A44}$$

We also consider the GL free energy. As shown in Eq. (13), the fluctuation contribution $\delta\mathcal{F}_{\text{fluct}}(t)$ is written as

$$\frac{\delta\mathcal{F}_{\text{fluct}}(t)}{\mathcal{F}_0} = k\frac{\delta\langle|\psi(\boldsymbol{r},t)|^2\rangle}{\psi_0^2}, \tag{A45}$$

where the superconducting fluctuation is given in Eq. (A44). The kinetic component of the GL free energy is written as

$$\frac{\delta\mathcal{F}_{\text{kin}}^{(\mu)}(t)}{\mathcal{F}_0} = e^{-kt/\mathcal{T}}Z_{\mu\mu}\left(0,\frac{t}{\mathcal{T}}\right) - 2x_{0\mu}e^{-kt/\mathcal{T}}Y_\mu\left(0,\frac{t}{\mathcal{T}}\right) + x_{0\mu}^2 e^{-kt/\mathcal{T}}X\left(0,\frac{t}{\mathcal{T}}\right) - e^{-kt/\mathcal{T}}W\left(\frac{t}{\mathcal{T}},0\right). \tag{A46}$$

### 3. Double pump-shot model

Next, we consider the double pump-shot model. The electric current density $\delta j_\mu(t,\Omega)$ is rewritten as

$$\delta j_\mu(t,\Omega) = e^{-kt/\mathcal{T}-\frac{(t-t_0)t_0}{t\mathcal{T}}x_0^2}\left[J_0 Y_\mu\left(\frac{t-t_0}{\mathcal{T}},\frac{t_0}{\mathcal{T}}\right) + \sigma_0\frac{E_{1\mu}^s(t)}{2\Omega\mathcal{T}}X\left(\frac{t-t_0}{\mathcal{T}},\frac{t_0}{\mathcal{T}}\right) + \sigma_0\sum_\nu\frac{E_{1\nu}^c(t)}{\Omega^2\mathcal{T}^2}Z_{\mu\nu}\left(\frac{t-t_0}{\mathcal{T}},\frac{t_0}{\mathcal{T}}\right)\right]$$
$$+ e^{-k(t-t_0)/\mathcal{T}}\left[J_0\tilde{Y}_\mu\left(\frac{t-t_0}{\mathcal{T}},0\right) + \sigma_0\frac{E_{1\mu}^s(t)}{2\Omega\mathcal{T}}\tilde{X}\left(\frac{t-t_0}{\mathcal{T}},0\right) + \sigma_0\sum_\nu\frac{E_{1\nu}^c(t)}{\Omega^2\mathcal{T}^2}\tilde{Z}_{\mu\nu}\left(\frac{t-t_0}{\mathcal{T}},0\right)\right]$$
$$- e^{-kt/\mathcal{T}-\frac{(t-t_0)t_0}{t\mathcal{T}}x_0^2}\left[J_0\tilde{Y}_\mu\left(\frac{t-t_0}{\mathcal{T}},\frac{t_0}{\mathcal{T}}\right) + \sigma_0\frac{E_{1\mu}^s(t)}{2\Omega\mathcal{T}}\tilde{X}\left(\frac{t-t_0}{\mathcal{T}},\frac{t_0}{\mathcal{T}}\right) + \sigma_0\sum_\nu\frac{E_{1\nu}^c(t)}{\Omega^2\mathcal{T}^2}\tilde{Z}_{\mu\nu}\left(\frac{t-t_0}{\mathcal{T}},\frac{t_0}{\mathcal{T}}\right)\right]$$
$$- e^{-k(t-t_0)/\mathcal{T}}\left[\sigma_0\frac{E_{1\mu}^s(t)}{2\Omega\mathcal{T}}X\left(\frac{t-t_0}{\mathcal{T}},0\right) + \sigma_0\frac{E_{1\mu}^c(t)}{\Omega^2\mathcal{T}^2}W\left(\frac{t-t_0}{\mathcal{T}},0\right)\right] + e^{-k(t-t_1)/\mathcal{T}}\sigma_0 E_{1\mu}V\left(\frac{t-t_1}{\mathcal{T}},\Omega\mathcal{T}\right). \tag{A47}$$

The case with $0 < t \leqslant t_0$ is the same situation corresponding to the single pump-shot model, which we have already considered in the above subsection. We then consider the region $t > t_0$. The fluctuation is written as

$$\frac{\delta\langle|\psi(\boldsymbol{r},t)|^2\rangle}{\psi_0^2} = e^{-kt/\mathcal{T}-\frac{(t-t_0)t_0}{t\mathcal{T}}x_0^2}X\left(\frac{t-t_0}{\mathcal{T}},\frac{t_0}{\mathcal{T}}\right) + e^{-k(t-t_0)/\mathcal{T}}\tilde{X}\left(\frac{t-t_0}{\mathcal{T}},0\right) - e^{-kt/\mathcal{T}-\frac{(t-t_0)t_0}{t\mathcal{T}}x_0^2}\tilde{X}\left(\frac{t-t_0}{\mathcal{T}},\frac{t_0}{\mathcal{T}}\right)$$
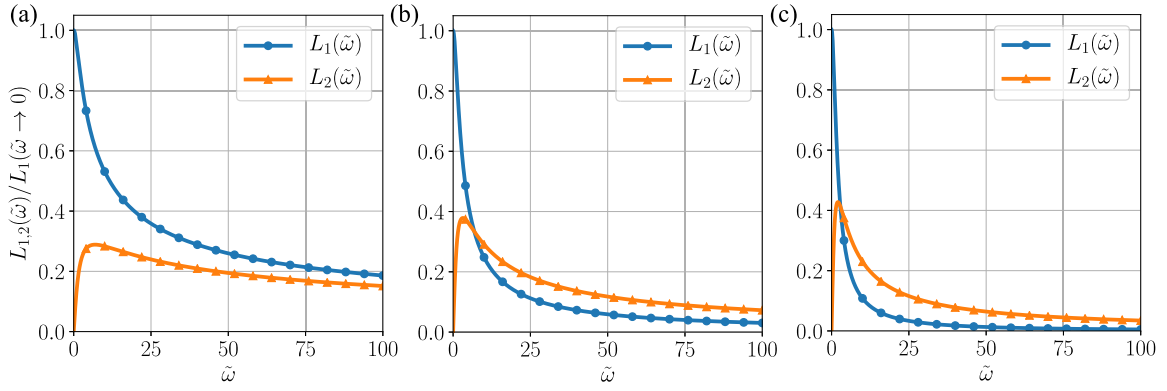$$- e^{-k(t-t_0)/\mathcal{T}}X\left(\frac{t-t_0}{\mathcal{T}},0\right). \tag{A48}$$

FIG. 8. Frequency dependences of $L_1$ and $L_2$ in the (a) three-, (b) two-, and (c) one-dimensional systems.

Next, we consider the GL free energy. The fluctuation contribution is the same as Eq. (A45). The kinetic component is

$$\frac{\delta\mathcal{F}_{\text{kin}}^{(\mu)}(t)}{\mathcal{F}_0} = e^{-kt/\mathcal{T} - \frac{(t-t_0)t_0}{t\mathcal{T}}x_0^2}Z_{\mu\mu}\left(\frac{t-t_0}{\mathcal{T}}, \frac{t_0}{\mathcal{T}}\right) + e^{-k(t-t_0)/\mathcal{T}}\tilde{Z}_{\mu\mu}\left(\frac{t-t_0}{\mathcal{T}}, 0\right) - e^{-kt/\mathcal{T} - \frac{(t-t_0)t_0}{t\mathcal{T}}x_0^2}\tilde{Z}_{\mu\mu}\left(\frac{t-t_0}{\mathcal{T}}, \frac{t_0}{\mathcal{T}}\right)$$

$$- e^{-k(t-t_0)/\mathcal{T}}W\left(\frac{t-t_0}{\mathcal{T}}, 0\right). \tag{A49}$$

## APPENDIX B: NUMERICAL EVALUATION FOR THE DIMENSIONLESS FUNCTIONS

The dimensionless functions defined in Appendix A are written in the following general form:

$$\int_0^\infty dx\,\mathcal{F}(x)e^{-\left(x-\frac{b}{2}\right)^2} = \int_{-\frac{b}{2}}^\infty dx\,\mathcal{F}\left(x+\frac{b}{2}\right)e^{-x^2} \tag{B1}$$

$$\simeq \frac{L_{\max}-L_{\min}}{2}\int_{-1}^1 dy\,\mathcal{F}\left(\frac{L_{\max}-L_{\min}}{2}y+\frac{L_{\max}+L_{\min}}{2}+\frac{b}{2}\right)e^{-\left(\frac{L_{\max}-L_{\min}}{2}y+\frac{L_{\max}+L_{\min}}{2}\right)^2}, \tag{B2}$$

where $L_{\max} > L_{\min}$ with the expressions

$$L_{\min} = -L, \quad L_{\max} = L\,(2L < b),$$

$$L_{\min} = -\frac{b}{2}, \quad L_{\max} = 2L - \frac{b}{2}\,(b < 2L). \tag{B3}$$

We assume that the function $\mathcal{F}(x)$ behaves asymptotically as a power function. Then, due to the presence of the exponential function, it is safe to choose $L \simeq 5$, since $e^{-5^2} \simeq 1.4 \times 10^{-11}$ are so small. We have used the Gauss-Legendre method [42] when we integrate the function numerically.

## APPENDIX C: TDGL THEORY IN EQUILIBRIUM

### 1. General formulation

We review the TDGL theory in an equilibrium system based on our formalism [29]. We assume the weak vector potential $A(t)$ without specifying its form. The superconducting fluctuation with the wave vector is obtained as

$$\langle|\psi_q(t)|^2\rangle = \frac{C}{\Gamma^2 V}\int_{-\infty}^t dt'\,\exp\left[-\frac{2}{\Gamma}\left(\frac{q^2}{4m}+a\right)(t-t')\right]$$

$$\times\left(1 + \frac{2e}{m\Gamma}\int_{t'}^t dt''\,q\cdot A(t'')\right) + O(A^2), \tag{C1}$$

where we used the random average given by Eq. (6). We can expand the representation of the current up to the first order of $A$ as

$$j(t) = \sum_q \frac{e}{mV}[q - 2eA(t)]\langle|\psi_q(t)|^2\rangle, \tag{C2}$$

$$\equiv j_0(t) + j_1(t) + O(A^2), \tag{C3}$$

where

$$j_0(t) = \frac{e}{mV}\sum_q q\langle|\psi_q(t)|^2\rangle_0 = 0, \tag{C4}$$

$$j_1(t) = \frac{e}{mV}\sum_q q\langle|\psi_q(t)|^2\rangle_1 - \frac{2e^2}{mV}A(t)\sum_q\langle|\psi_q(t)|^2\rangle_0, \tag{C5}$$

$$\equiv j_1^P(t) + j_1^D(t). \tag{C6}$$

We have treated the vector potential as perturbation. We note that the integrand of $j_0(t)$ with respect to $q$ is an odd function. The subscripts "0" and "1" mean the perturbation order of $A$. "$P$" and "$D$" denote "paramagnetic" and "diamagnetic" contributions. We abbreviate the argument $r$ since the current is spatially uniform.

Performing the Fourier transformation, the current is rewritten as

$$j_\mu(\omega) = K_{\mu\nu}(\omega)A_\nu(\omega), \tag{C7}$$

$$\equiv \left(K_{\mu\nu}^P(\omega) + K_{\mu\nu}^D(\omega)\right)A_\nu(\omega), \tag{C8}$$

where

$$K_{\mu\nu}^{P}(\omega) = \frac{2e^2 C}{m^2 \Gamma^3 V^2} \sum_{\boldsymbol{q}} q_\mu q_\nu \frac{g(\boldsymbol{q})^2}{1 - i\omega g(\boldsymbol{q})}, \tag{C9}$$

$$= \frac{2e^2 C}{m^2 \Gamma^3 V^2} \sum_{\boldsymbol{q}} q_\mu q_\nu g(\boldsymbol{q})^2 \sum_{n=0}^{\infty} [i\omega g(\boldsymbol{q})]^n, \tag{C10}$$

$$K_{\mu\nu}^{D}(\omega) = -\frac{2e^2 C}{m \Gamma^2 V^2} \delta_{\mu\nu} \sum_{\boldsymbol{q}} g(\boldsymbol{q}). \tag{C11}$$

The paraconductivity $\sigma_{\mu\nu}(\omega)$ is then obtained by

$$\sigma_{\mu\nu}(\omega) = \frac{K_{\mu\nu}(\omega)}{i\omega}. \tag{C12}$$

Note the relation $K_{\mu\nu}^{P}(\omega)|_{n=0} = -K_{\mu\nu}^{D}(\omega)$. The total kernel can be rewritten as

$$K_{\mu\nu}(\omega) = \frac{2e^2 C}{im \Gamma^2 V^2 \omega} \delta_{\mu\nu} \sum_{\boldsymbol{q}} \sum_{n=1}^{\infty} \frac{[i\omega g(\boldsymbol{q})]^{n+1}}{n+1}. \tag{C13}$$

When we define a dimensionless frequency $\tilde{\omega} = \frac{\omega}{\gamma_1} = \frac{\Gamma\omega}{2a}$, the response kernel is further rewritten as

$$K_{\mu\nu}(\omega) = \frac{e^2 C}{im \Gamma V a} \frac{1}{\tilde{\omega}} \delta_{\mu\nu} I(\tilde{\omega}), \tag{C14}$$

where

$$I(\tilde{\omega}) = \int \frac{d\boldsymbol{q}}{(2\pi)^d} \left[ -i\tilde{\omega} \frac{4ma}{\boldsymbol{q}^2 + 4ma} - \ln\left(1 - i\tilde{\omega} \frac{4ma}{\boldsymbol{q}^2 + 4ma}\right) \right]. \tag{C15}$$

In the following, we perform the $\boldsymbol{q}$-integral for each dimension.

### 2. Three-dimensional system

The ac paraconductivity for $d = 3$ is given by

$$\sigma_{\mu\nu}(\omega) = \frac{e^2 C \sqrt{m}}{3\pi V} a^{-1/2} \delta_{\mu\nu} \left[ L_1\left(\frac{\Gamma\omega}{2a}\right) + iL_2\left(\frac{\Gamma\omega}{2a}\right) \right], \tag{C16}$$

where

$$L_1(\tilde{\omega}) = \frac{1}{\tilde{\omega}^2} \left[ 2 - \sqrt{2(\sqrt{1 + \tilde{\omega}^2} + 1)} + \tilde{\omega}\sqrt{2(\sqrt{1 + \tilde{\omega}^2} - 1)} \right], \tag{C17}$$

$$L_2(\tilde{\omega}) = \frac{1}{\tilde{\omega}^2} \left[ -3\tilde{\omega} + \sqrt{2(\sqrt{1 + \tilde{\omega}^2} - 1)} + \tilde{\omega}\sqrt{2(\sqrt{1 + \tilde{\omega}^2} + 1)} \right]. \tag{C18}$$

The dependence of these quantities with respect to $\tilde{\omega}$ is shown in Fig. 8(a).

### 3. Two-dimensional system

The ac paraconductivity for $d = 2$ is given by

$$\sigma_{\mu\nu}(\omega) = \frac{e^2 C}{2\pi V} a^{-1} \delta_{\mu\nu} \left[ L_1\left(\frac{\Gamma\omega}{2a}\right) + iL_2\left(\frac{\Gamma\omega}{2a}\right) \right], \tag{C19}$$
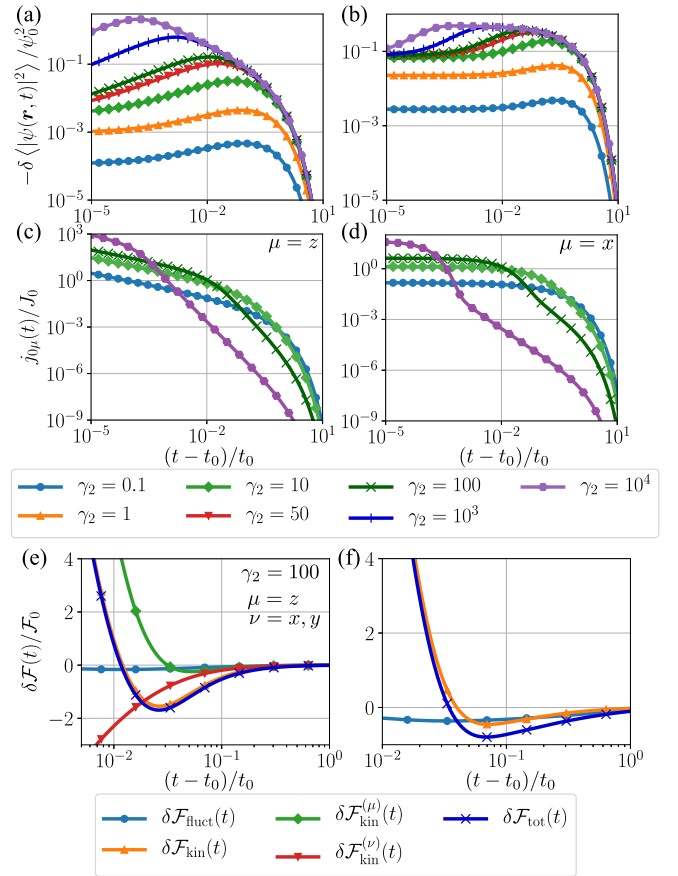


FIG. 9. Time dependences of the (a), (b) superconducting fluctuation, the (c), (d) excited current and the (e), (f) GL free energy with the logarithmic time scale in the double pump-shot model. The panels (a), (c), (e) are for three-dimensional systems and (b), (d), (f) for one-dimensional system. We take the parameter as $\gamma_1 = 1$ and (e), (f) $\gamma_2 = 100$ to compare with the results of the single pump-shot model ($t_0 = 1$). $\mu$ and $\nu$ used in (e) have the same meanings as Fig. 4(a). The normalized constants are defined by $\psi_0^2 = \frac{Ct_0}{\Gamma^2 V} \left(\frac{2m\Gamma}{t_0}\right)^{d/2}$, $J_0 = \frac{eCt_0}{m\Gamma^2 V} \left(\frac{2m\Gamma}{t_0}\right)^{\frac{d+1}{2}}$ and $\mathcal{F}_0 = \frac{C}{2\Gamma} \left(\frac{2m\Gamma}{t_0}\right)^{d/2}$.

where

$$L_1(\tilde{\omega}) = \frac{1}{\tilde{\omega}^2} \left[ \tilde{\omega} \arctan \tilde{\omega} - \frac{1}{2} \ln(1 + \tilde{\omega}^2) \right], \tag{C20}$$

$$L_2(\tilde{\omega}) = \frac{1}{\tilde{\omega}^2} \left[ \arctan \tilde{\omega} + \frac{1}{2} \tilde{\omega} \ln(1 + \tilde{\omega}^2) - \tilde{\omega} \right]. \tag{C21}$$

These functions are shown in Fig. 8(b).

### 4. One-dimensional system

The ac paraconductivity for $d = 1$ is given by

$$\sigma_{\mu\nu}(\omega) = \frac{e^2 C}{2V\sqrt{m}} a^{-3/2} \delta_{\mu\nu} \left[ L_1\left(\frac{\Gamma\omega}{2a}\right) + iL_2\left(\frac{\Gamma\omega}{2a}\right) \right], \tag{C22}$$

where

$$L_1(\tilde{\omega}) = \frac{1}{\tilde{\omega}^2} \left[ -2 + \sqrt{2(\sqrt{1 + \tilde{\omega}^2} + 1)} \right], \tag{C23}$$

$$L_2(\tilde{\omega}) = \frac{1}{\tilde{\omega}^2} \left[ \tilde{\omega} - \sqrt{2(\sqrt{1 + \tilde{\omega}^2} - 1)} \right]. \tag{C24}$$

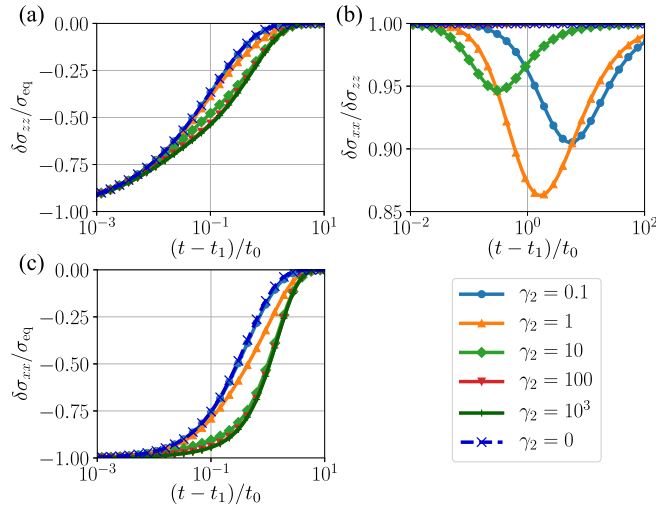These functions are shown in Fig. 8(c).

FIG. 10. Time dependences of the nonequilibrium component of (a) the dc paraconductivity and (b) anisotropy parameter $\delta\sigma_{xx}/\delta\sigma_{zz}$ in the three-dimensional systems (double pump-shot model). The vertical axis in (a) is normalized by the equilibrium component of the paraconductivity $\sigma_{\mathrm{eq}} = \frac{e^2 C}{3\pi V}\sqrt{\frac{m}{a}}$. Note that the vertical axis in (b) is measured from the unity (isotropic limit). The dc paraconductivity for one-dimensional systems is also shown in (c), where the values are also normalized by $\sigma_{\mathrm{eq}} = \frac{e^2 C}{2V\sqrt{ma^3}}$. We have taken $\gamma_1 = 1$ and $t_1 = 1.1$ with the time unit $t_0 (= 1)$.

We note that the vertical axis in Fig. 8 is normalized by the $L_1(\tilde{\omega} \to 0)$. For all the dimensions, $L_1$ ($L_2$), which is the real (imaginary) part of paraconductivity, is an even (odd) function of frequency. These quantities satisfy the Kramers-Kronig relation. As seen from Fig. 8, the behavior in the
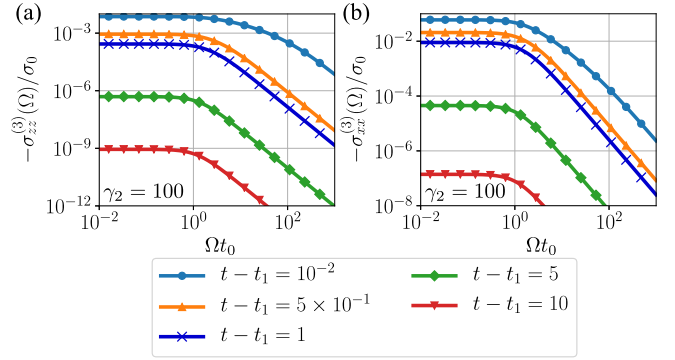


FIG. 11. Frequency dependence of the ac paraconductivity $\sigma^{(3)}$ at several different times in the (a) three- and (b) one-dimensional systems (double pump-shot model). In these figures, we have taken $\gamma_1 = 1$, $\gamma_2 = 100$, and $t_1 = 1.1$ with the unit time $t_0 (= 1)$. The normalization constant is defined by $\sigma_0 = \frac{4e^2 C}{m\Gamma^2 V}\left(\frac{2m\Gamma}{t_0}\right)^{d/2}$.

low-frequency region is sharper for the lower-dimensional system.

## APPENDIX D: ADDITIONAL DATA FOR THE DOUBLE PUMP-SHOT MODEL IN THREE- AND ONE-DIMENSIONAL SYSTEMS

While the double pump-shot model in the two-dimensional system is studied in the main text, here we show the results in three dimensions and one dimension to make the data complete. Figure 9 shows the time dependence of the fluctuation, current density, and free energy, which are plots similar to Fig. 5. Figures 10 and 11 show the nonequilibrium component of the dc and ac paraconductivities, respectively, which correspond to Figs. 6 and 7 of the main text.

[1] S. Iwai, M. Ono, A. Maeda, H. Matsuzaki, H. Kishida, H. Okamoto, and Y. Tokura, Phys. Rev. Lett. **91**, 057401 (2003).

[2] L. Perfetti, P. A. Loukakos, M. Lisowski, U. Bovensiepen, H. Berger, S. Biermann, P. S. Cornaglia, A. Georges, and M. Wolf, Phys. Rev. Lett. **97**, 067402 (2006).

[3] H. Okamoto, H. Matsuzaki, T. Wakabayashi, Y. Takahashi, and T. Hasegawa, Phys. Rev. Lett. **98**, 037401 (2007).

[4] D. Fausti, R. I. Tobey, N. Dean, S. Kaiser, A. Dienst, M. C. Hoffmann, S. Pyon, T. Takayama, H. Takagi, and A. Cavalleri, Science **331**, 189 (2011).

[5] Y. H. Wang, H. Steinberg, P. Jarillo-Herrero, and N. Gedik, Science **342**, 453 (2013).

[6] L. Stojchevska, I. Vaskivskyi, T. Mertelj, P. Kusar, D. Svetin, S. Brazovskii, and D. Mihailovic, Science **344**, 177 (2014).

[7] J. Zhang, X. Tan, M. Liu, S. W. Teitelbaum, K. W. Post, F. Jin, K. A. Nelson, D. N. Basov, W. Wu, and R. D. Averitt, Nat. Mater. **15**, 956 (2016).

[8] C. Giannetti, M. Capone, D. Fausti, M. Fabrizio, and F. Parmigiani, Adv. Phys. **65**, 58 (2016).

[9] W. Hu, S. Kaiser, D. Nicoletti, C. R. Hunt, I. Gierz, M. C. Hoffmann, M. Le Tacon, T. Loew, B. Keimer, and A. Cavalleri, Nat. Mater. **13**, 705 (2014).

[10] R. Mankowsky, A. Subedi, M. Först, S. O. Mariager, M. Chollet, H. T. Lemke, J. S. Robinson, J. M. Glownia, M. P.

Minitti, A. Frano, M. Fechner, N. A. Spaldin, T. Loew, B. Keimer, A. Georges, and A. Cavalleri, Nature (London) **516**, 71 (2014).

[11] S. Kaiser, C. R. Hunt, D. Nicoletti, W. Hu, I. Gierz, H. Y. Liu, M. Le Tacon, T. Loew, D. Haug, B. Keimer, and A. Cavalleri, Phys. Rev. B **89**, 184516 (2014).

[12] D. Nicoletti, E. Casandruc, Y. Laplace, V. Khanna, C. R. Hunt, S. Kaiser, S. S. Dhesi, G. D. Gu, J. P. Hill, and A. Cavalleri, Phys. Rev. B **90**, 100503(R) (2014).

[13] M. Mitrano, A. Cantaluppi, D. Nicoletti, S. Kaiser, A. Perucchi, S. Lupi, P. Di Pietro, D. Pontiroli, M. Riccò, S. R. Clark, D. Jaksch, and A. Cavalleri, Nature (London) **530**, 461 (2016).

[14] A. Cantaluppi, M. Buzzi, G. Jotzu, D. Nicoletti, M. Mitrano, D. Pontiroli, M. Riccò, A. Perucchi, P. Di Pietro, and A. Cavalleri, Nat. Phys. **14**, 837 (2018).

[15] F. Giusti, A. Marciniak, F. Randi, G. Sparapassi, F. Boschini, H. Eisaki, M. Greven, A. Damascelli, A. Avella, and D. Fausti, Phys. Rev. Lett. **122**, 067002 (2019).

[16] S. J. Denny, S. R. Clark, Y. Laplace, A. Cavalleri, and D. Jaksch, Phys. Rev. Lett. **114**, 137001 (2015).

[17] J. I. Okamoto, A. Cavalleri, and L. Mathey, Phys. Rev. Lett. **117**, 227001 (2016).

[18] M. A. Sentef, A. F. Kemper, A. Georges, and C. Kollath, Phys. Rev. B **93**, 144506 (2016).

[19] M. Kim, Y. Nomura, M. Ferrero, P. Seth, O. Parcollet, and A. Georges, Phys. Rev. B **94**, 155152 (2016).

[20] M. Knap, M. Babadi, G. Refael, I. Martin, and E. Demler, Phys. Rev. B **94**, 214504 (2016).

[21] M. A. Sentef, Phys. Rev. B **95**, 205111 (2017).

[22] M. Babadi, M. Knap, I. Martin, G. Refael, and E. Demler, Phys. Rev. B **96**, 014512 (2017).

[23] Y. Murakami, N. Tsuji, M. Eckstein, and P. Werner, Phys. Rev. B **96**, 045125 (2017).

[24] G. Mazza and A. Georges, Phys. Rev. B **96**, 064515 (2017).

[25] D. M. Kennes, E. Y. Wilner, D. R. Reichman, and A. J. Millis, Nat. Phys. **13**, 479 (2017).

[26] A. Nava, C. Giannetti, A. Georges, E. Tosatti, and M. Fabrizio, Nat. Phys. **14**, 154 (2018).

[27] D. M. Kennes and A. J. Millis, Phys. Rev. B **96**, 064507 (2017).

[28] G. Chiriacò, A. J. Millis, and I. L. Aleiner, Phys. Rev. B **98**, 220510(R) (2018).

[29] A. Larkin and V. Varlamov, *Theory of Fluctuations in Superconductors* (Oxford University Press, Oxford, 2005).

[30] See, for example, M. Sigrist and K. Ueda, Rev. Mod. Phys. **63**, 239 (1991).

[31] L. P. Gor'kov and G. M. Eliashberg, Zh. Eksp. Teor. Fiz. **54**, 612 (1968) [Sov. Phys. JETP **27**, 328 (1968)].

[32] N. B. Kopnin, *Theory of Nonequilibrium Superconductivity* (Oxford University Press, Oxford, 2001).

[33] Y. Lemonik and A. Mitra, Phys. Rev. B **98**, 214514 (2018).

[34] A. Schmid, Phys. Rev. **180**, 527 (1969).

[35] R. Wakatsuki, Y. Saito, S. Hoshino, Y. M. Itahashi, T. Ideue, M. Ezawa, Y. Iwasa, and N. Nagaosa, Sci. Adv. **3**, e1602390 (2017).

[36] R. Wakatsuki and N. Nagaosa, Phys. Rev. Lett. **121**, 026601 (2018).

[37] S. Hoshino, R. Wakatsuki, K. Hamamoto, and N. Nagaosa, Phys. Rev. B **98**, 054510 (2018).

[38] P. C. Hohenberg and B. I. Halperin, Rev. Mod. Phys. **49**, 435 (1977).

[39] A. F. Volkov and Sh. M. Kogan, Zh. Eksp. Teor. Fiz. **65**, 2038 (1973) [Sov. Phys. JETP **38**, 1018 (1974)].

[40] R. A. Barankov and L. S. Levitov, Phys. Rev. Lett. **96**, 230403 (2006).

[41] S. Uchida, Physica C **282–287**, 12 (1997).

[42] See, for example, F. B. Hildebrand, *Introduction to Numerical Analysis* (Dover, New York, 1987).